Plastic–Damage Analysis of Koyna Dam in Different Damping Mechanisms with Dam–Water Interaction

O. Omidi & V. Lotfi
Amirkabir University of Technology, Iran

S. Valliappan
University of New South Wales, Australia

SUMMARY:
Seismic fracture response of Koyna dam is examined by a plastic–damage model in different damping mechanisms. The plastic–damage model implemented in three-dimensional space was proposed by Lee and Fenves in 1998. It was founded on the combination of non-associated multi-hardening plasticity and isotropic damage theory. In this study, utilizing the HHT scheme as an implicit operator, responses of Koyna dam as a benchmark problem for the seismic fracture researches, are compared due to constant and damage-dependent damping mechanisms. It is concluded that employing the damage-dependent damping mechanism leads to more extensive damages and also predicts more reliable crack patterns in comparison with the constant damping mechanism. Furthermore, considering dam–reservoir interaction intensifies the existing differences between the results of the two different damping mechanisms. The results emphasize that water compressibility and damping mechanism are two important issues in seismic safety evaluation of concrete gravity dams.

Keywords: plastic–damage; gravity dam; damage-dependent damping; dam–water interaction; seismic safety

1. INTRODUCTION

There are numerous high concrete dams throughout the world. However, their fracture responses under strong ground excitations have been monitored and reported only in a few cases. Koyna dam in India experienced a destructive earthquake in 1967. The Koyna earthquake with a maximum acceleration of around 0.5g caused major damage to the dam including horizontal cracks on the upstream and downstream in a number of its non-overflow monoliths (Chopra and Chakrabarti 1973).

In order to assess the seismic safety of concrete dams, nonlinear models simulating crack propagation within the dam body need to be employed. To accurately simulate the degradation in the mechanical properties of concrete, the use of continuum damage mechanics is necessary. However, concrete also experiences some irreversible deformations during unloading such that the continuum damage theories alone cannot be used successfully. Therefore, concrete can be realistically simulated by two separate material mechanical processes: damage and plasticity. Plasticity theory has been widely used to describe the concrete behavior (Menetrey and Willam 1995; Grassl *et al.* 2002). The main characteristic of these models is a yield surface that includes pressure sensitivity, path sensitivity, non-associative flow rule, and work or strain hardening. However, these investigations fail to address the degradation of the material stiffness due to micro-cracking. On the other hand, the continuum damage theory has also been employed to include the mechanical effect of the progressive micro-cracking and strain softening are represented by a set of internal variables (i.e. decrease of the stiffness) at the macroscopic level (Loland 1980; Mazars and Pijaudier-Cabot 1989; Valliappan *et al.* 1991; Cervera et al. 1995; Valliappan *et al.* 1996). The use of coupling between damage and plasticity has been found to be necessary for capturing the observed experimental-based behavior of concrete (Lemaitre 1985; Lubliner *et al.* 1989; Lee and Fenves 1998a, 2001; Menzel *et al.* 2002; Salari *et al.* 2004; Wu *et al.* 2006; Grassl and Jirasek 2006; Cicekli *et al.* 2007; Voyiadjis *et al.* 2008; Abu Al-Rub and Voyiadjis 2009).

However, only a limited number of studies have been performed to investigate the dynamic behavior of concrete dams using a plastic–damage constitutive law (Lee and Fenves 1998b; Wu and Li 2007; Sarkar *et al.* 2007). The plastic–damage model, which was originally proposed by Lubliner *et al.* in 1989 and later on modified by Lee and Fenves in 1998, is employed herein to investigate the nonlinear dynamic behavior of concrete dams in two different damping mechanisms. It should be emphasized that the available implementation of the model is limited to 2-D plane stress state. This study utilizes the model in 3-D formulation implemented in a special finite element program, SNACS (Omidi 2010) for the seismic application to Koyna dam in 3-D modelling.

2. PLASTIC–DAMAGE CONSTITUTIVE LAW

The constitutive relations of the plastic–damage model are fully described by Lee and Fenves in (Lee and Fenves 1998a, 2001). In the 3-D implementation of the model, the apex's singularity of the linear potential function proposed and used by Lee and Fenves needs to be avoided. Moreover, singularities of the yield surface must be taken into account. Computational aspects of the treated model in 3-D space along with the stress update algorithm are thoroughly discussed in (Omidi and Lotfi 2010a). However for the sake of clarity and completeness of this paper, a brief description is presented herein.

2.1. Framework of plastic–damage model

In order to describe full states of damage on the elastic stiffness in a three-dimensional stress state, a 4^{th}-rank tensor needs to be used (Voyiadjis *et al.* 2008). However, scalar degradation damage models are useful for practical applications due to simplicity (Grassl and Jirasek 2006; Nguyen and Korsunsky 2008; Saritas and Filippou 2009). Furthermore, a scalar representation for damage on the stiffness can be significantly enhanced to predict various states of damage when it is combined with plasticity theory. The fundamental relations of a rate-independent plastic–damage model as the backbone model of its corresponding rate-dependent extension can be expressed as follows.

2.1.1. Stress-strain relationship

The strain tensor, $\boldsymbol{\varepsilon}$, is decomposed into the elastic part, $\boldsymbol{\varepsilon}^{\mathrm{e}}$, and the plastic part, $\boldsymbol{\varepsilon}^{\mathrm{p}}$. The elastic part is defined as the recoverable portion in the total strain. The stress, $\boldsymbol{\sigma}$, and the effective stress, $\bar{\boldsymbol{\sigma}}$, are as:

$$\boldsymbol{\sigma} = (1-D)\bar{\boldsymbol{\sigma}} \;; \quad \bar{\boldsymbol{\sigma}} = \mathbf{E}_0 : (\boldsymbol{\varepsilon} - \boldsymbol{\varepsilon}^{\mathrm{p}}) \tag{2.1}$$

where $\mathbf{E}_0$ is a rank-four elastic stiffness tensor. The degradation damage variable, D, is used to represent a scalar form of damage in the elastic stiffness. To determine the required effective stress tensor, the evolution law for the plastic strain tensor needs to be established. The evolution law of the plastic–damage variables (i.e., κ_{t} and κ_{c}) playing the role of hardening variables, in addition to the plastic strains, is necessary to be specified. These evolution laws are given by:

$$\dot{\boldsymbol{\varepsilon}}^{\mathrm{p}} = \dot{\lambda}\,\nabla_{\bar{\boldsymbol{\sigma}}}\Phi \;; \quad \dot{\boldsymbol{\kappa}} = \dot{\lambda}\,\mathbf{H}(\bar{\boldsymbol{\sigma}}, \boldsymbol{\kappa}) \;; \quad \boldsymbol{\kappa} = \begin{pmatrix} \kappa_{\mathrm{t}} & \kappa_{\mathrm{c}} \end{pmatrix}^{\mathrm{T}} \tag{2.2}$$

where Φ is a scalar potential function; λ is a nonnegative function referred to as the plastic consistency parameter and $\mathbf{H}$, which actually represents hardening components, is derived considering plastic dissipation. Furthermore, the damage variables in tension and compression, which are denoted by D_{t} and D_{c} respectively, are explicit functions of the plastic–damage variables in tension and compression introduced above. Since the model is accurately capable of capturing the two major damage phenomena, the uniaxial tensile and compressive ones, multi-dimensional degradation behavior can be possibly evaluated by interpolating between these two main damage variables as:

$$D = 1 - (1 - D_{\mathrm{c}}(\kappa_{\mathrm{c}}))(1 - s\,D_{\mathrm{t}}(\kappa_{\mathrm{t}})) \tag{2.3}$$

in which s is called the stiffness recovery parameter such that $0 \le s \le 1$ and used to include the elastic stiffness recovery during elastic unloading process from tension to compression:

$$s\,(\hat{\bar{\boldsymbol{\sigma}}}) = s_0 + (1-s_0)\,r(\hat{\bar{\boldsymbol{\sigma}}})\;; \quad r(\hat{\bar{\boldsymbol{\sigma}}}) = \left(\sum_{\mathrm{i}=1}^{3}\langle\hat{\bar{\sigma}}_{\mathrm{i}}\rangle\right) \Big/ \left(\sum_{\mathrm{i}=1}^{3}\left|\hat{\bar{\sigma}}_{\mathrm{i}}\right|\right)\;; \qquad 0 \le r(\hat{\bar{\boldsymbol{\sigma}}}) \le 1 \tag{2.4}$$

where s_0 is a minimum value for s usually set to zero; r is a weight factor and $\langle x\rangle$ is the ramp function (i.e., $\langle x\rangle = (x + |x|)/2$).

2.1.2. Non-associated flow rule

The Drucker–Prager hyperbolic function is employed here as the plastic potential function:

$$\Phi = \sqrt{\beta_{\mathrm{H}}^2 + 2\bar{J}_2} + \alpha_{\mathrm{p}}\bar{I}_1\;; \quad \beta_{\mathrm{H}} = \varepsilon_0\,\alpha_{\mathrm{p}}\,f_{\mathrm{t0}} \tag{2.5}$$

where $\bar{I}_1$ and $\bar{J}_2$ are the first and second invariants of the effective stress tensor; the parameter α_{p} should be calibrated to give proper dilatancy; f_{t0} is the maximum uniaxial tensile strength. Moreover, ε_0, which is called the eccentricity parameter, controls how the function approaches the asymptote (i.e., the linear function). Based on theory of plasticity, loading/unloading conditions are derived from the Kuhn–Tucker relations which are given in terms of the yield function $F(\bar{\boldsymbol{\sigma}}, \boldsymbol{\kappa})$ and the plastic consistency parameter as $\dot{\lambda} \ge 0$; $F(\bar{\boldsymbol{\sigma}}, \boldsymbol{\kappa}) \le 0$; $\dot{\lambda} F(\bar{\boldsymbol{\sigma}}, \boldsymbol{\kappa}) = 0$. Lee and Fenves modified the yield function in the Barcelona model (Lubliner *et al.* 1989) to include two cohesion variables for tension and compression. In fact, the tensile and compressive cohesion variables in the yield function are necessarily included due to different tensile and compressive yield strengths.

$$\begin{aligned} F(\bar{\boldsymbol{\sigma}}, \boldsymbol{\kappa}) &= f(\bar{\boldsymbol{\sigma}}, \boldsymbol{\kappa}) - c_{\mathrm{c}}(\boldsymbol{\kappa}) \\ f(\bar{\boldsymbol{\sigma}}, \boldsymbol{\kappa}) &= \frac{1}{1-\alpha}\left[\sqrt{3\bar{J}_2} + \alpha\,\bar{I}_1 + \beta(\boldsymbol{\kappa})\,\langle\hat{\bar{\sigma}}_{\max}\rangle - \gamma\,\langle -\hat{\bar{\sigma}}_{\max}\rangle\right] \end{aligned} \tag{2.6}$$

where $\hat{\bar{\sigma}}_{\max}$ is the maximum principal stress; α is a parameter evaluated on the basis of an initial shape of the yield function and γ is a coefficient affecting only the states of tri-axial compression. Moreover, β, which is a constant in the Barcelona model, was later modified by Lee and Fenves as:

$$\beta(\boldsymbol{\kappa}) = \frac{c_{\mathrm{c}}(\kappa_{\mathrm{c}})}{c_{\mathrm{t}}(\kappa_{\mathrm{t}})}(1-\alpha) - (1+\alpha) \tag{2.7}$$

in which, c_{t} and c_{c} are tensile and compressive cohesion variables, respectively.

2.2. Large crack opening/closing

The evolution relation used for the damage variables needs to be modified to simulate large cracking in such a continuum model (Lee and Fenves 1998b). The crack opening/closure mechanism becomes similar to a discrete crack after that a large damage is sustained in tension region, i.e. $\kappa_{\mathrm{t}} > \kappa_{\mathrm{cr}}$ where κ_{cr} is an empirical value usually close to unity. At such a tensile damage level, the evolution of plastic strain caused by tensile damage is stopped and the plastic strain rate is computed as:

$$\dot{\boldsymbol{\varepsilon}}^{\mathrm{p}} = (1-r)\,\dot{\bar{\boldsymbol{\varepsilon}}}^{\mathrm{p}}\;; \quad r = r(\hat{\bar{\boldsymbol{\sigma}}}) \tag{2.8}$$

in which, $\tilde{\boldsymbol{\varepsilon}}^{\mathrm{p}}$ is referred to as the intermediate plastic strain; r is a weight function and $\tilde{\boldsymbol{\sigma}}$ is also the intermediate effective stress defined as:

$$\tilde{\boldsymbol{\sigma}} = \mathbf{E}_0 : (\boldsymbol{\varepsilon} - \tilde{\boldsymbol{\varepsilon}}^{\mathrm{p}}) \in \left\{ \tilde{\boldsymbol{\sigma}} \mid F(\tilde{\boldsymbol{\sigma}}, \boldsymbol{\kappa}) \le 0 \right\} \tag{2.9}$$

In this condition, the intermediate plastic strain rate is given by $\dot{\tilde{\boldsymbol{\varepsilon}}}^{\mathrm{p}} = \dot{\lambda} \nabla_{\tilde{\boldsymbol{\sigma}}} \Phi$. To make the effective stress based on the plastic strain admissible in the stress space, it is necessary to employ a new damage variable denoted by D_{cr} at the crack damage corrector which makes the evaluated effective stress return back onto the yield surface. This is determined by the plastic consistency condition for a continued loading such that $F((1-D_{\mathrm{cr}})\,\bar{\boldsymbol{\sigma}}, \boldsymbol{\kappa}) = 0$ from which D_{cr} is obtained as $D_{\mathrm{cr}} = 1 - c_{\mathrm{c}}(\boldsymbol{\kappa}) / f(\bar{\boldsymbol{\sigma}}, \boldsymbol{\kappa})$. The stiffness degradation variable is redefined considering large cracking as follows:

$$D = 1 - (1 - D_{\mathrm{c}})(1 - s\,D_{\mathrm{t}})(1 - s\,D_{\mathrm{cr}}) \tag{2.10}$$

The numerical implementation and the stress update algorithm modified to consider large cracking possibilities have been detailed in (Omidi and Lotfi 2010, 2012).

2.3. Rate-dependent extension

Employing visco-plastic regularization reduces the dependency on mesh refinement and alignment (Lee and Fenves 1998b). Furthermore, convergence difficulties in material constitutive laws simulating softening behavior and stiffness degradation can be partially overcome by using its rate-dependent extension. Both plastic strain and degradation variable are regularized herein by adding viscosity with the Duvaut-Lions regularization. The visco-plastic strain rate tensor, $\dot{\boldsymbol{\varepsilon}}^{\mathrm{vp}}$, and the viscous stiffness degradation variable, D^{v}, for the visco-plastic system are defined, respectively by:

$$\dot{\boldsymbol{\varepsilon}}^{\mathrm{vp}} = \frac{1}{\mu}(\boldsymbol{\varepsilon}^{\mathrm{p}} - \boldsymbol{\varepsilon}^{\mathrm{vp}}) \;; \quad \dot{D}^{\mathrm{v}} = \frac{1}{\mu}(D - D^{\mathrm{v}}) \tag{2.11}$$

where μ, which is called the viscosity parameter, shows the relaxation time of the visco-plastic model; $\boldsymbol{\varepsilon}^{\mathrm{p}}$ and D are the plastic strain and stiffness degradation variable computed in the inviscid backbone model. The governing stress-strain relation for the rate-dependent model would be as:

$$\boldsymbol{\sigma} = (1 - D^{\mathrm{v}})\,\mathbf{E}_0 : (\boldsymbol{\varepsilon} - \boldsymbol{\varepsilon}^{\mathrm{vp}}) \tag{2.12}$$

2.4. Visco-elastic damping stress

The visco-elastic damping stress in the constant damping mechanism is expressed as the following:

$$\boldsymbol{\chi}(\dot{\boldsymbol{\varepsilon}}) = \beta_{\mathrm{R}}\,\mathbf{E}_0 : \dot{\boldsymbol{\varepsilon}} \tag{2.13}$$

where β_{R} is the coefficient of viscous damping and calibrated to provide a damping ratio at one natural vibration period. This kind of damping introduces artificial damping forces as cracks open with large relative velocity and the damping force then restrains the crack opening by transferring artificial stresses across the crack. To remedy this problem, some investigators set the damping term to zero upon cracking of an element or use the tangent stiffness matrix (Horii and Chen 2003). On the other hand, a nonlinear form of visco-elastic damping called damage-dependent damping is based consistently on the elastic properties accounting for degradation damage (Lee and Fenves 1998b) as:

$$\boldsymbol{\chi}(\boldsymbol{\varepsilon}, \dot{\boldsymbol{\varepsilon}}) = \beta_{\mathrm{R}}\,(1 - D)\mathbf{E}_0 : \dot{\boldsymbol{\varepsilon}} \tag{2.14}$$

3. TIME INTEGRATION SCHEME WITH DAM–RESERVOIR INTERACTION

The Lagrangian–Eulerian formulation, in which displacement and pressure are unknown variables for dam and reservoir, respectively, is utilized to construct the governing coupled equations. The equations of motion may be written as follows for the discretized dam under ground acceleration:

$$\mathbf{M}\,\ddot{\mathbf{U}} + \mathbf{P}(\mathbf{u},\dot{\mathbf{u}}) = \mathbf{R}^{\mathrm{st}} + \mathbf{Q}^{\mathrm{T}}\,\mathbf{p} \quad ; \qquad \ddot{\mathbf{U}} = \ddot{\mathbf{u}} + \mathbf{J}\,\mathbf{a}_{\mathrm{g}} \tag{3.1}$$

where $\mathbf{M}$ is the mass matrix of dam body; $\mathbf{u}$, $\dot{\mathbf{u}}$ and $\ddot{\mathbf{u}}$ represent the nodal vectors of the displacement, velocity and acceleration relative to the ground motion, respectively; $\ddot{\mathbf{U}}$ is the vector of absolute nodal acceleration; $\mathbf{P}$ denotes the restoring force vector; $\mathbf{Q}$ is often referred to as interaction or coupling matrix; $\mathbf{p}$ represents the vector of nodal hydrodynamic pressures and $\mathbf{R}^{\mathrm{st}}$ is the static loads vector; $\mathbf{a}_{\mathrm{g}}$ denotes the vector of ground accelerations and $\mathbf{J}$ is a matrix with each of the three rows equal to a 3×3 identity matrix. It is noted that in the current implementation, the element's restoring force vector, $\mathbf{P}^{e}$, is given by the integral of the total stress including damping stress over the element volume. The mass-proportional term for the damping matrix has been omitted, because it would provide some artificial numerical stability during time marching process. Furthermore, one can apply Galerkin method to the wave equation and impose related boundary conditions to obtain the following relation for the discretized reservoir domain:

$$\mathbf{G}\,\ddot{\mathbf{p}} + \mathbf{L}\,\dot{\mathbf{p}} + \mathbf{H}\,\mathbf{p} = -\rho\,\mathbf{Q}\,\ddot{\mathbf{U}} \tag{3.2}$$

where $\mathbf{G}$, $\mathbf{L}$ and $\mathbf{H}$ are called generalized mass, damping and stiffness matrices, respectively. In order to construct the coupled equations set of the system consistently, the governing equations for the dam and reservoir are restated as the following, respectively:

$$\mathbf{M}\,\ddot{\mathbf{U}} + \mathbf{F}(\mathbf{u},\dot{\mathbf{u}},\mathbf{p}) = \mathbf{R}^{\mathrm{st}} \quad ; \qquad \mathbf{F}(\mathbf{u},\dot{\mathbf{u}},\mathbf{p}) = \mathbf{P}(\mathbf{u},\dot{\mathbf{u}}) - \mathbf{Q}^{\mathrm{T}}\,\mathbf{p} \tag{3.3}$$

$$\mathbf{G}\,\ddot{\mathbf{p}} + \mathbf{F}'(\mathbf{p},\dot{\mathbf{p}}) = -\rho\,\mathbf{Q}\,\ddot{\mathbf{U}} \quad ; \qquad \mathbf{F}'(\mathbf{p},\dot{\mathbf{p}}) = \mathbf{L}\,\dot{\mathbf{p}} + \mathbf{H}\,\mathbf{p} \tag{3.4}$$

Now one could set up the following coupled equations:

$$\begin{pmatrix} \mathbf{M} & \mathbf{0} \\ \rho\,\mathbf{Q} & \mathbf{G} \end{pmatrix} \begin{pmatrix} \ddot{\mathbf{u}} \\ \ddot{\mathbf{p}} \end{pmatrix} + \begin{pmatrix} \mathbf{F} \\ \mathbf{F}' \end{pmatrix} = \begin{pmatrix} \mathbf{R} \\ \mathbf{R}' \end{pmatrix} \tag{3.5}$$

where $\mathbf{R} = \mathbf{R}^{\mathrm{st}} - \mathbf{M}\,\mathbf{J}\,\mathbf{a}_{\mathrm{g}}$ and $\mathbf{R}' = -\rho\,\mathbf{Q}\,\mathbf{J}\,\mathbf{a}_{\mathrm{g}}$. Considering $\bar{\mathbf{u}}$, $\dot{\bar{\mathbf{u}}}$ and $\ddot{\bar{\mathbf{u}}}$ as total displacement, velocity and acceleration vectors with the following definitions:

$$\bar{\mathbf{u}} = \begin{pmatrix} \mathbf{u} \\ \mathbf{p} \end{pmatrix} \; ; \; \dot{\bar{\mathbf{u}}} = \begin{pmatrix} \dot{\mathbf{u}} \\ \dot{\mathbf{p}} \end{pmatrix} \; ; \; \ddot{\bar{\mathbf{u}}} = \begin{pmatrix} \ddot{\mathbf{u}} \\ \ddot{\mathbf{p}} \end{pmatrix} \tag{3.6}$$

Denoting $\bar{\mathbf{M}}$ as the total mass matrix, Eqn. (3.5) could be written in a more compact form as:

$$\bar{\mathbf{M}}\,\ddot{\bar{\mathbf{u}}} + \bar{\mathbf{F}} = \bar{\mathbf{R}}\,; \qquad \bar{\mathbf{M}} = \begin{pmatrix} \mathbf{M} & \mathbf{0} \\ \rho\,\mathbf{Q} & \mathbf{G} \end{pmatrix} \; ; \; \bar{\mathbf{F}} = \begin{pmatrix} \mathbf{F} \\ \mathbf{F}' \end{pmatrix} \; ; \; \bar{\mathbf{R}} = \begin{pmatrix} \mathbf{R} \\ \mathbf{R}' \end{pmatrix} \tag{3.7}$$

Numerical damping associated with the time-stepping schemes used for integrating second-order systems of equations over time stabilizes the numerical integration by damping out the unwanted high frequency modes. For the Newmark method, numerical damping also affects the lower modes and

reduces the accuracy of integration scheme from second order to first order. For the HHT method, numerical damping affects only the higher modes and always maintains second-order accuracy. Larger numerical damping values are usually necessary for problems involving rigid body rotational motion and dynamic contact/impact (Lee and Fenves 2001). Utilizing the HHT integration scheme, the discrete form of the governing equilibrium equation, Eqn. (3.7), is written at the time step $n+1$ as:

$$\bar{\mathbf{M}}\,\ddot{\bar{\mathbf{u}}}_{n+1} + \bar{\mathbf{F}}(\bar{\mathbf{u}}_{n+\varphi}, \dot{\bar{\mathbf{u}}}_{n+\varphi}) - \bar{\mathbf{R}}_{n+\varphi} = \mathbf{0} \tag{3.8}$$

where $\varphi = 1+\alpha$ and α is the free parameter controlling the amount of the numerical dissipation, which is increased by decreasing α. The recommended range for α is $[-1/3, 0]$ to achieve unconditional stability, second-order accuracy and good high-frequency dissipative characteristics. It is noted that the generalized mid-point scheme is only used for the equations of motion (i.e., $\bar{\mathbf{u}}_{n+\varphi}$ and $\dot{\bar{\mathbf{u}}}_{n+\varphi}$) and the applied force, $\bar{\mathbf{R}}_{n+\varphi}$. Since employing the generalized mid-point scheme in the stress computation does not have robust numerical performance (Simo 1991), the stresses needed for the restoring force vector, $\mathbf{P}_{n+\varphi}$, is integrated based on the shifted backward-Euler scheme (Lee and Fenves 2001), in which the internal variables are directly computed at $t_{n+\varphi}$ rather than t_{n+1}. It should be noted that the shifted scheme becomes the original method in $[t_{n+\varphi-1}, t_{n+\varphi}]$.

4. FRACTURE RESPONSE OF KOYNA DAM

This section focuses on the seismic fracture response of Koyna dam which has been broadly examined by many investigators as the main validation of their proposed concrete models (Bhattacharjee and Leger 1993; Lee and Fenves 1998b; Guanglun *et al.* 2000; Mirzabozorg and Ghaemian 2005; Calayir and Karaton 2005). Koyna dam is a 103 m high concrete gravity dam located in India and constructed in 1963. It was subjected to the 1967 earthquake of magnitude 6.5 and was severely damaged (Chopra and Chakrabarti 1973). Its scaled model was also experimentally tested by Hall in 1988.

4.1. Mesh, model parameters and loading

The simulation is based on the 3-D modeling of a slice of a typical monolith depicted in Fig. 4.1a. The cracked configuration experimentally observed is also shown in this figure (Hall 1988). The 8-node isoparametric solid and fluid elements are utilized to discretize the dam and reservoir domains, respectively as illustrated in Fig. 4.1b. The material properties are as: $E_0 = 30.0$ GPa, $\nu = 0.2$, $f_t' = 2.9$ MPa, $f_c' = -24.1$ MPa, $G_t = 200$ N/m, $G_c = 20000$ N/m and $\mu = 0.1\Delta t$. Moreover, $\Delta t = 0.005$ sec and $\alpha = -0.3$ are selected as the analysis parameters. The thickness of the slice is one meter and the dam body is assumed to be in a state of plane stress. The length of the reservoir simulated in the model is 2.5 times of the reservoir height while the reservoir bottom is assumed to be partially reflective with the wave reflection coefficient equal to 0.85. The unit weights of concrete and water are assumed as 25.8 and 9.81 kN/m^3, respectively. The stiffness proportional damping factor is computed such that 3 percent damping is being captured for the fundamental vibration period.
The static loads are applied at negative range of time in 10 increments each before the earthquake excitation is employed. Afterwards, 10 sec of the horizontal and vertical components of the 1967 earthquake records shown in Fig. 4.1c are applied to the base of the dam and reservoir starting at time zero. The time integration is performed for 15 sec of which the last 5 sec is free vibration.

4.2. Results for damage-dependent damping mechanism

Fig. 4.2 shows the stream displacement at the left corner of the crest relative to the ground motion while positive horizontal displacement is in the downstream direction. The four different times marked in Fig. 4.2 are focused to track the damage evolution in the dam body (Fig. 4.3).

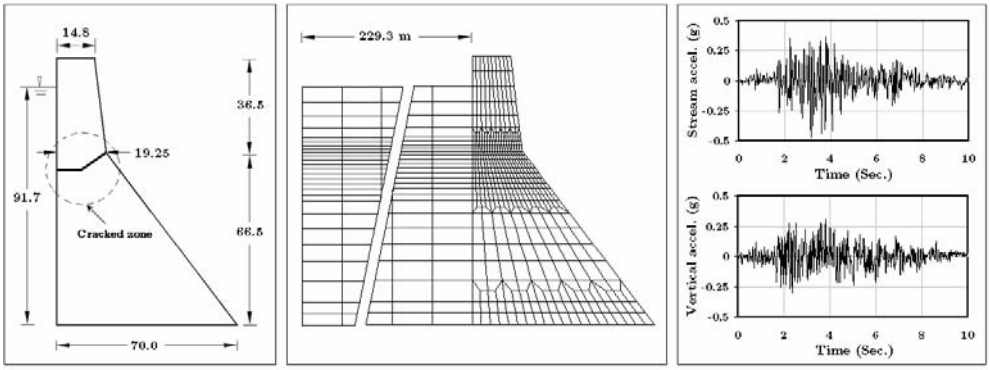

Figure 4.1. Koyna gravity dam: (a) geometry of the tallest monolith (unit: m) along with cracked zone experimentally observed (Hall 1988), (b) mesh and (c) the 1967 Koyna earthquake components

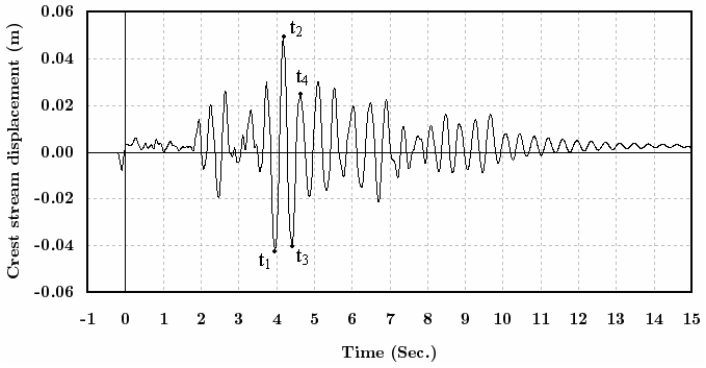

Figure 4.2. Crest stream displacement history with damage-dependent damping mechanism

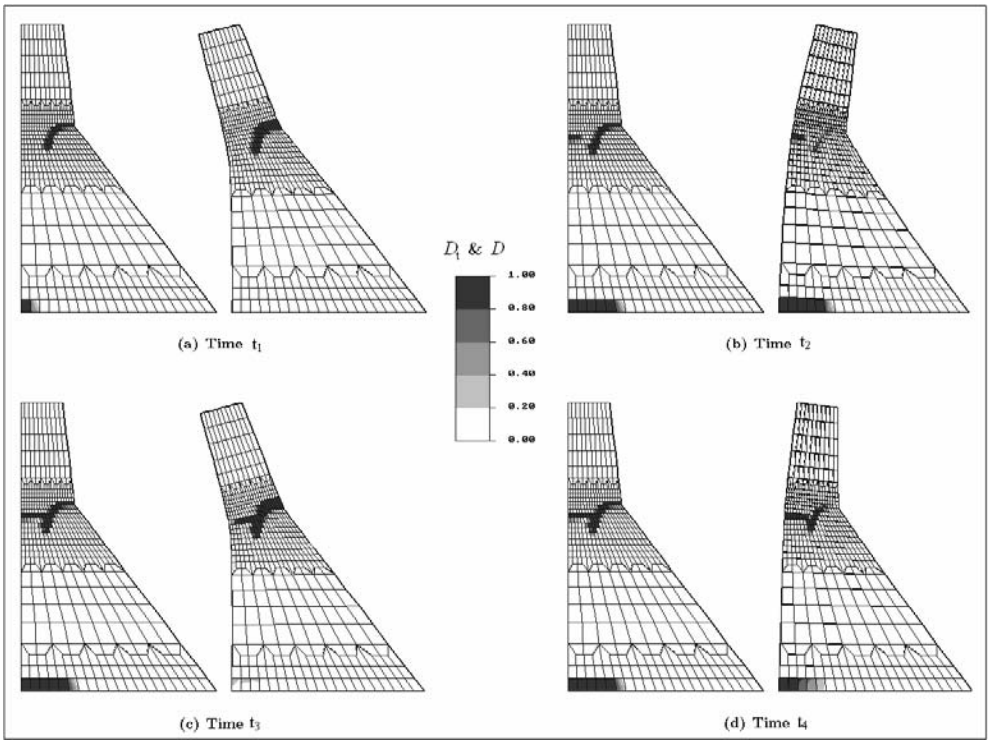

Figure 4.3. Evolution of tensile damage, D_t (left) and degradation variable, D (right) in the analysis with dam–water interaction using damage-dependent damping mechanism

As observed in Fig. 4.3a, near the downstream change of slope, a crucial damage has occurred and the localized band of damaged elements is formed by time t_1. Curving down due to the rocking motion of the upper block, this downstream crack propagates toward the upstream direction. When the dam displaces toward downstream at time t_2, some damaged elements appear at the base (Fig. 4.3b). This crack propagates into the dam along the lowest layer of the elements at the base due to the rigid foundation. Furthermore, at this major deformation to the downstream direction (i.e., time t_2), the load is reversed and as it is now expected, the crack having occurred at downstream closes ,which obviously shows the stiffness recovery on this region due to compressive stresses. At this time, a horizontal crack propagating toward the curved part of the downstream crack is formed. As noticed, the tensile damage has very well localized on just one layer of the elements along the upstream face. At time t_3, the dam moves toward upstream again and as illustrated in Fig. 4.3c, all cracks have occurred in the body by this time and from now on the upper block of the dam oscillating back and forth during the rest of the earthquake remains stable while the upstream and downstream cracks alternatively close and open. At time t_4, the damages captured in Fig. 4.3d shows that the crack at the base remains stable and does not propagate further.

4.3. Results for constant damping mechanism

Employing the constant damping mechanism, Koyna dam is reanalyzed herein. Fig. 4.4a shows the distribution of tensile damage at the end of the simulation. Similar to the analysis carried out with damage-dependent damping mechanism, three major cracks developing during the earthquake are at the base of the dam, at the downstream change of slope and at the upstream face near to the upper part of the dam. The captured crack pattern when the analysis employs the constant damping mechanism is quite different from the corresponding one while the damage-dependent damping is employed in the analysis. Actually, this kind of damping utilizing the linear form of visco-elastic damping stress creates artificial damping forces as cracks open with large relative velocity and the damping forces then restrains the crack opening by transferring artificial stresses across the crack. In some previous studies, Koyna dam has been analyzed using constant damping but considering a reduced tensile strength along with reduced fracture energy in tension (Calayir and Karaton 2005]. Under these circumstances, one would expect the dam to undergo more damages. In these analyses, the tensile strength and the fracture energy are assumed as $f_t' = 1.5\,\text{MPa}$ and $G_t = 150\,\text{N/m}$, respectively (Fig. 4.4b) although more severe damage has occurred in the dam body in comparison with the original material data, no clear macro crack can be observed and the upper cracked zones are not localized while the crack profile also differs from the experiment.

4.4. Water compressibility effects

In order to assess the influence of water compressibility on the cracking response of the dam, the dam–reservoir interaction is taken into account by the widely-used added mass approximation. Results are compared for damage-dependent damping and constant damping in Fig. 4.4c and 4.4d.

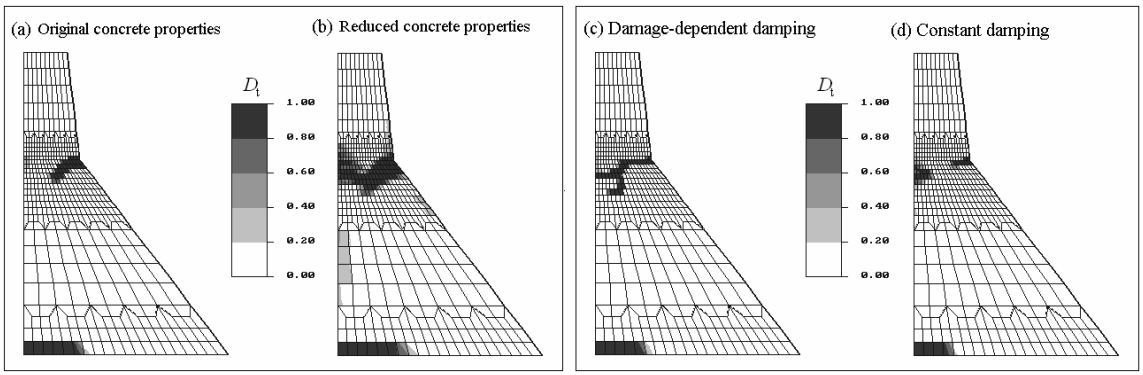

Figure 4.4. Damage distribution using constant damping (left) and using the added mass approximation (right)

5. CONCLUSIONS

A special finite element program called SNACS has been developed for the non-linear seismic evaluation of concrete dams based on a plastic–damage approach. The model implemented for 3-D stress state had been successfully employed in its 2-D version for the analysis of concrete gravity dams with 2-D plane stress state by Lee and Fenves. The constitutive model objectively represents localization of damage caused by strain softening. Damping is consistently accounted for using the reduced stiffness caused by damage degradation. Utilizing the damage-dependent and constant damping mechanisms, SNACS program is employed in analyzing Koyna gravity dam and comparing the results with the available experimental observation. The comparison between the cases of different damping mechanisms reveals major differences in the results. Seismic cracking response of Koyna dam indicates that the dam remains stable at all times during earthquake excitation. The evolution of damage in the dam during the earthquake is consistent with the observed cracking in the dam when the damage-dependent damping mechanism is being utilized. After cracks form near the change in downstream slope at both faces, the upper portion of the dam rocks nearly as a rigid body. Moreover, the damaged zone is localized, generally one element wide, demonstrating that the localization behavior caused by strain softening is represented satisfactorily in the plastic–damage model implemented in three dimensional spaces of present study. This had been previously shown in two-dimensional representations by other researchers. On the other hand, when the constant damping mechanism is employed in the analysis, the resulting crack profile has no agreement with that reported experimentally. Besides, the upper cracked zone at the slope change in this option is not localized.

Furthermore, the seismic fracture response of Koyna dam is also conducted when the effect of the dam–reservoir interaction is taken into account. Results of the analysis are compared to the case when the dam–reservoir interaction was represented by added masses. It is found that including dam–reservoir interaction gives a crack pattern that is closer to the damaged configuration observed in its experimental counterpart. The predicted damage zone is different from that of the case when the dam–reservoir interaction is approximated using the added mass approach. The results emphasize that damping mechanism and water compressibility are two issues significantly affecting nonlinear design of concrete dams. These factors need to be properly addressed in dam design practices when general-purpose programs such as ABAQUS, ANSYS, ADINA, etc. are employed in a seismic safety analysis.

ACKNOWLEDGMENTS

A part of this research became possible while the first author had his visit to the University of New South Wales, Australia. He wishes to thank Professor Nasser Khalili for his help during the visit. Moreover, the supports of the elite National Foundation and the Ministry of Science, Research and Technology of Iran are greatly appreciated.

REFERENCES

Abu Al-Rub, R.K. and Voyiadjis, G.Z. (2009). Gradient-enhanced coupled plasticity–anisotropic damage model for concrete fracture: computational aspects and applications. *International Journal of Damage Mechanics.* **18**, 115-154.

Bhattacharjee, S.S. and Leger, P. (1993). Seismic cracking and energy dissipation in concrete gravity dams. *Earthquake Engineering and Structural Dynamics*. **22**, 991-1007.

Calayir, Y. and Karaton, M. (2005). Seismic fracture analysis of concrete gravity dams including dam–reservoir interaction. *Computers and Structures.* **83**, 1595-1606.

Cervera, M., Oliver, J. and Faria, R. (1995). Seismic evaluation of concrete dams via continuum damage models. *Earthquake Engineering and Structural Dynamics.* **24**, 1225-1245.

Chopra, A.K. and Chakrabarti. P. (1973). The Koyna earthquake and damage to Koyna dam. *Bulletin of the Seismological Society of America.* **63**, 381-397.

Cicekli, U., Voyiadjis, G.Z. and Abu Al-Rub, R.K. (2007). A plasticity and anisotropic damage model for plain concrete. *International Journal of Plasticity.* **23**, 1874-1900.

Grassl, P. and Jirasek, M. (2006). Damage–plastic model for concrete failure. *International Journal of Solids and Structures.* **43**, 7166-7196.

Grassl, P., Lundgren K. and Gylltoft, K. (2002). Concrete in compression: a plasticity theory with a novel hardening law. *International Journal of Solids and Structures.* **39**, 5205-5223.

Guanglun, W., Pekau, O.A., Chuhan, Z. and Shaomin, W. (2000). Seismic fracture analysis of concrete gravity dams based on nonlinear fracture mechanics. *Engineering Fracture Mechanics.* **65,** 67-87.

Hall, J.F. (1988). The dynamic and earthquake behavior of concrete dams: Review of experimental behavior and observational evidence. *Soil Dynamics and Earthquake Engineering.* **7**, 57-121.

Horii, H. and Chen, S.C. (2003). Computational fracture analysis of concrete gravity dams by crack-embedded elements: toward an engineering evaluation of seismic safety. *Engineering Fracture Mechanics.* **70**, 1029-1045.

Lee, J. and Fenves, G.L. (1998a). A plastic–damage model for cyclic loading of concrete structures. *Journal of Engineering Mechanics, ASCE*. **124**, 892-900.

Lee, J. and Fenves, G.L. (1998b). A plastic–damage model for earthquake analysis of dams. *Earthquake Engineering and Structural Dynamics*. **27**, 937-956.

Lee, J. and Fenves, G.L. (2001). A return-mapping algorithm for plastic–damage models: 3-D and plane stress formulation. *International Journal for Numerical Methods in Engineering*, 50: 487-506.

Lemaitre,J. (1985). Coupled elasto-plasticity and damage constitutive equations. *Computer Methods in Applied Mechanics and Engineering.* **51**, 31-49.

Loland, K.E. (1980). Continuous damage model for load-response estimation of concrete. *Cement Concrete Research.* **10**, 395-402.

Lubliner, J., Oliver, J., Oller, S. and Onate, E. (1989). A plastic–damage model for concrete. *International Journal of Solids and Structures.* **25**, 299-326.

Mazars, J. and Pijaudier-Cabot, G. (1989). Continuum damage theory: application to concrete. *Journal of Engineering Mechanics.* **115**, 345-365.

Menetrey, Ph. and Willam, K.J. (1995). Triaxial failure criterion for concrete and its generalization. *ACI Structural Journal.* **92**, 311-318.

Menzel, A., Ekh, M., Steinmann, P. and Runesson, K. (2002). Anisotropic damage coupled to plasticity: modeling based on the effective configuration concept. *International Journal of Numerical Methods in Engineering.* **54**, 1409-1430.

Mirzabozorg, H. and Ghaemian, M. (2005). Nonlinear behavior of mass concrete in three-dimensional problems using a smeared crack approach. *Earthquake Engineering and Structural Dynamics*. **34**, 247-269.

Nguyen, G.D. and Korsunsky, A.M. (2008). Development of an approach to constitutive modeling of concrete: isotropic damage coupled with plasticity. *International Journal of Solids and Structures.* **45**, 5483-5501.

Omidi O. and Lotfi V. (2012) .Continuum large cracking in a rate-dependent plastic–damage model for cyclic-loaded concrete structures. *International Journal for Numerical and Analytical Methods in Geomechanics*. Accepted for publication.

Omidi, O. (2010) .SNACS: A program for Seismic Nonlinear Analysis of Concrete Structures. Department of Civil and Environmental Engineering, Amirkabir University of Technology, Tehran, Iran.

Omidi, O. and Lotfi, V. (2007). Application of pseudo–symmetric technique for seismic analysis of concrete arch dams. *Fourth International Conference on Fluid–Structure Interaction.* **Vol I:** 153-162.

Omidi, O. and Lotfi, V. (2010a). Finite element analysis of concrete structures using plastic–damage model in 3-D implementation. *International Journal of Civil Engineering.* **8:3**, 187-203.

Omidi, O. and Lotfi, V. (2010b). Numerical analysis of cyclically loaded concrete under large tensile strains by the plastic–damage model. *Scientia Iranica, Transaction A: Civil Engineering.* **17**, 194-208.

Salari, M.R., Saeb, S., Willam, K.J., Patchet, S.J. and Carrasco, R.C. (2004). A coupled elastoplastic damage model for geomaterials. *Computer Methods in Applied Mechanics and Engineering.* **193**, 2625-2643.

Saritas, A. and Filippou, F.C. (2009). Numerical integration of a class of 3d plastic–damage concrete models and condensation of 3d stress-strain relations for use in beam finite elements. *Engineering Structures.* **31**, 2327-2336.

Simo, J.C. (1991). Algorithm for static and dynamics multiplicative plasticity that preserve the classical return-mapping schemes of the infinitesimal theory. *Computer Methods in Applied Mechanics and Engineering.* **99**, 61-112.

Valliappan, S., Murti, V. and Zhang, W. (1991). Finite element analysis of anisotropic damage mechanics problems. *Engineering Fracture Mechacnis.* **35**, 1061-1071.

Valliappan, S., Yazdchi, M. and Khalili, N. (1996). Earthquake analysis of gravity dams based on damage mechanics concept. *International Journal of Numerical and Analytical Methods in Geomechanics.* **20**, 725-751.

Voyiadjis, G.Z., Taqieddin, Z.N. and Kattan, P.I. (2008). Anisotropic damage–plasticity model for concrete. *International Journal of Plasticity.* **24**, 1946-1965.

Wu, J.Y. and Li, J. (2007). Unified plastic–damage model for concrete and its applications to dynamic nonlinear analysis of structures. Structual Engineering Mechanics. **25**, 519-540.

Wu, J.Y., Li, J. and Faria, R. (2006). An energy release rate-based plastic–damage model for concrete. *International Journal of Solids and Structures.* **43**, 583-612.